Composites Science and Technology 70 (2010) 1360–1367

Contents lists available at ScienceDirect

Composites Science and Technology

journal homepage: www.elsevier.com/locate/compscitech

Failure analysis and the optimal toughness design of carbon nanotube-reinforced composites

Y.L. Chen [a], B. Liu [a,*], X.Q. He [b], Y. Huang [c], K.C. Hwang [a]

[a] AML, Department of Engineering Mechanics, Tsinghua University, Beijing 100084, China
[b] Department of Building and Construction, City University of Hong Kong, Tat Chee Avenue, Kowloon, Hong Kong, China
[c] Depts. of Civil and Environmental Eng. and Mechanical Eng., Northwestern Univ., Evanston, IL 60208, United States

ARTICLE INFO

Article history:
Received 4 January 2010
Received in revised form 23 March 2010
Accepted 18 April 2010
Available online 24 April 2010

Keywords:
A. CNT-reinforced composites
B. Fracture toughness
B. Bridging effect
C. Multiscale modeling

ABSTRACT

The combined analysis of the fracture toughness enhancement of carbon nanotube (CNT)-reinforced composites is herein carried out on the basis of atomistic simulation, shear-lag theory and facture mechanics. It is found that neither longer reinforced CNTs nor stronger CNT/matrix interfaces can definitely lead to the better fracture toughness of these composites. In contrast, the optimal interfacial chemical bond density and the optimal CNT length are those making the failure mode just in the transition from CNT pull-out to CNT break. To verify our theory, an atomic/continuum finite element method (FEM) is applied to investigate the fracture behavior of CNT-reinforced composites with different interfacial chemical bond densities. Our analysis shows that the optimal interfacial chemical bond density for (6,6) CNTs is about 5–10% and that increasing the CNT length beyond 100 nm does not further improve fracture toughness, but can easily lead to the self-folding and clustering of the CNTs. The proposed theoretical model is also applicable to short fiber-reinforced composites.

1. Introduction

Carbon nanotubes (CNTs) possess exceptionally superior physical and mechanical properties, such as high strength and low density, and therefore hold great promise for employment as reinforcements in advanced composites [1–10]. However, experimental and numerical studies show that the performance of such composites depends critically on the CNT/matrix interfacial characteristics [11–13]. Interface strength and interface length are two of the most important factors that affect the mechanical properties of CNT-reinforced composites and therefore have drawn the attention of many researchers.

Prior experimental and numerical studies of CNT-reinforced composite materials have shown only minor improvements in their mechanical properties [14–19], primarily because the CNTs are often easily pulled out due to weak van der Waals interactions between the CNTs and the matrix [19–21]. Therefore, research efforts are currently aimed at strengthening this interface. Some experimental and numerical studies have demonstrated that strengthening the interface by covalent bonds can improve the mechanical properties of CNT-reinforced composites significantly [11,16]. Thus, researchers have tried in various ways, such as non-ionic surfactant and ion bombardment [11,16,22,23], to form covalent bonds between CNTs and the matrix. At the same time, theoretical studies of fiber-reinforced composites have shown that the interface length is also an important influential factor. Researchers have thus attempted to prepare CNTs as long as possible. The longest CNTs produced to date are in the order of centimeters [24,25], but the mass production of CNTs of this length at low cost remains a huge challenge.

Such research efforts also prompt an important question: do longer CNTs and stronger interfaces definitely result in CNT-reinforced composites with better mechanical properties? If the answer is no, what is the optimal CNT length and interface strength? This paper aims to provide answers to these two questions by investigating the effects of CNT length and interface strength on the fracture toughness of CNT-reinforced composites.

2. Roadmap for the failure analysis of CNT-reinforced composites

In CNT-reinforced composites with macroscopic cracks, CNTs of a high degree of strength can retard crack propagation, and a fracture zone bridged by CNTs at the crack tip is formed, as shown in Fig. 1a. This toughening effect of bridging CNTs is equivalent to that of nonlinear springs connecting the upper and lower crack surfaces, as shown in Fig. 1b. The force–displacement relation for these springs can be obtained by studying the

* Corresponding author. Tel.: +86 10 62786194.
E-mail address: liubin@tsinghua.edu.cn (B. Liu).

0266-3538/$ - see front matter © 2010 Elsevier Ltd. All rights reserved.
doi:10.1016/j.compscitech.2010.04.015

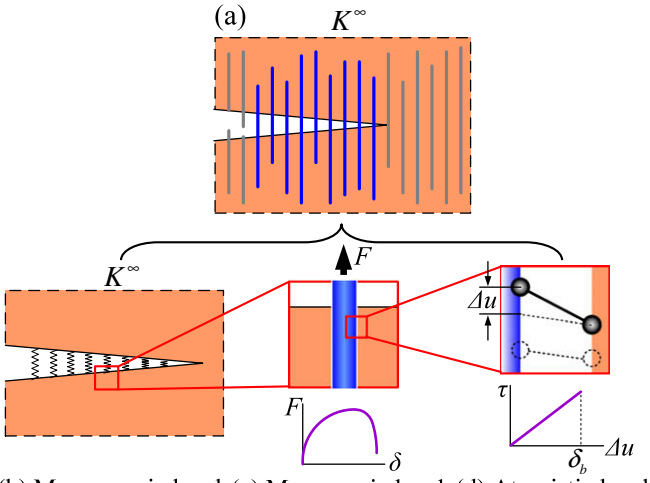

Fig. 1. Schematic diagram of three-level failure analysis models: (a) fracture zone bridged with CNTs at the crack tip; (b) macroscopic-level model with equivalent bridging nonlinear springs; (c) mesoscopic-level model for studying CNT-fiber failure and obtaining the force–displacement relation of equivalent nonlinear spring; (d) atomistic-level failure model for characterizing CNT/matrix interfacial bond breaking.

pulling force F and pull-out displacement δ of a single CNT, as shown in Fig. 1c. This F–δ curve depends on the interfacial atomic bond properties, i.e., on the interaction between atoms, as shown in Fig. 1d. Therefore, CNT-reinforced composites have three failure mode levels: a bond break mode at the atomistic level, CNT fiber failure mode at the mesoscopic level and macroscopic crack propagation at the macroscopic level. To better understand and optimize the fracture toughness of CNT-reinforced composites, this paper presents three-level failure analysis. We first adopt continuum mechanics to investigate CNT fiber and macroscopic-level failure in Section 3, and carry out the fracture toughness optimization analysis in Section 4, then employ the combined atomic/continuum finite element method (FEM) to investigate atomic bond and CNT fiber-level failure in Section 5. Our conclusions are summarized in the last section.

3. Continuum analysis on the fracture toughness of CNT-reinforced composites

It should be pointed out that, there are already a large amount of continuum mechanics studies on the fracture toughness of fiber-reinforced composites, especially the widely-used shear-lag theory [26–36]. Chon and Sun [27] studied stress distribution along a single reinforcing fiber of a randomly oriented chopped-fiber composite on assumption of perfect bonding. Lawrance [28] assumed the stiffness of the fiber is lower than that of the matrix and investigated fiber pull-out from an elastic matrix. For ceramic composites, Marchall et al. [29] studied the cracking in brittle-matrix, Hutchinson and Jensen [30] treated debonding process as a mode 2 crack to study fiber debonding and pull-out, and based on these studies, Budiansky et al. [31] accounted for an interfacial debonding resistance and studied the effects of debonding and initial stress on overall composite toughness. Many of these models are also applicable to CNT-reinforced composites. However, for the completeness and convenience to readers, the related analysis is briefly presented in this section.

According to the shear-lag theory, the interaction between CNTs and the matrix that results from the chemical bonds shown in Fig. 2 is shear stress, which is related to the relative displacement between the CNT fiber and the matrix Δu. A bond break occurs when Δu reaches the critical shear displacement δ_b, which depends only on the type of functionalization bond at the interface, whereas the corresponding interface strength τ_b also depends on the interface bond density. The interface shear stress τ is assumed to be proportional to the relative displacement Δu, i.e.,

$$\tau(x) = k\Delta u(x) = k[u_m(x) - u_f(x)] \tag{1}$$

where $k = \tau_b/\delta_b$ is the shear stiffness of the interface, and $u_m(x)$ and $u_f(x)$ are the axial or x-direction displacements of the matrix and the CNT fiber respectively.

Suppose the CNT and the matrix are both linear elastic, with the Young's modulus E_f and E_m, respectively. A representative volume element (RVE) including a single CNT with embedded length L and diameter d, as shown in Fig. 2, is adopted for analysis. With the balance conditions of the fiber and the matrix, the shear stress distribution can be derived [28]

$$\tau(x) = F\sqrt{\frac{\tau_b}{C\delta_b}}\cdot\frac{\frac{1}{E_mA_m}\cosh\left(x\sqrt{\frac{C\tau_b}{\delta_b}}\right) + \frac{1}{E_fA_f}\cosh\left[(x-L)\sqrt{\frac{C\tau_b}{\delta_b}}\right]}{\sinh\left(L\sqrt{\frac{C\tau_b}{\delta_b}}\right)} \tag{2}$$

where A_f and A_m are the cross-section areas of the CNT and the matrix in the RVE, F is the pulling force, and C depends on the material constants and geometry parameters as

$$C = \pi d\left(\frac{1}{E_fA_f} + \frac{1}{E_mA_m}\right) \tag{3}$$

The distribution of the axial normal stress in the CNT can also be derived as

$$\sigma(x) = \frac{1}{A_f}\left[F - \int_0^x \pi d\tau(x)\mathrm{d}x\right] \tag{4}$$

The two main fiber-level failure modes are usually interfacial debonding and fiber break.

(i) Critical condition for CNT fiber break

CNT break occurs when the maximum axial normal stress reaches CNT strength σ_f^b, and the corresponding critical pulling force is

$$F_{\max}^{\sigma} = \sigma_f^b A_f \tag{5}$$

(ii) Critical condition for interfacial debonding

According to Eq. (2) and noting $E_fA_f > E_mA_m$ for CNT-reinforced composites, the maximum shear stress on the interface can be found at the $x = L$ position, and

$$\tau(x)|_{\max} = \tau(L) = F\sqrt{\frac{\tau_b}{C\delta_b}}\cdot\frac{\frac{1}{E_mA_m}\cosh\left(L\sqrt{\frac{C\tau_b}{\delta_b}}\right) + \frac{1}{E_fA_f}}{\sinh\left(L\sqrt{\frac{C\tau_b}{\delta_b}}\right)} \tag{6}$$

When the maximum shear stress reaches the interface strength τ_b, the interfacial chemical bonds break, and the CNT is pulled out. The corresponding critical pulling force is

$$F_{\max}^{\tau} = \frac{\sqrt{C\tau_b\delta_b}\sinh\left(L\sqrt{\frac{C\tau_b}{\delta_b}}\right)}{\frac{1}{E_mA_m}\cosh\left(L\sqrt{\frac{C\tau_b}{\delta_b}}\right) + \frac{1}{E_fA_f}} \tag{7}$$

Together with Eqs. (5) and (7), the transition condition between the pull-out and break failure modes is

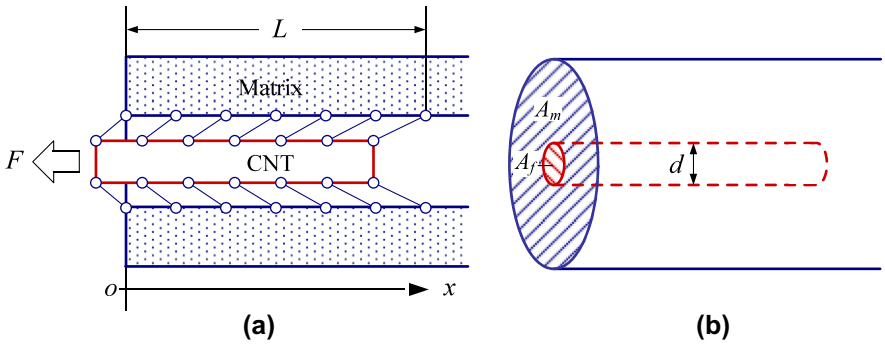

Fig. 2. Schematic diagram of shear-lag model for the interactions between the CNT and the matrix (a) and the geometric parameters (b).

$$\begin{cases} \dfrac{\sigma_f^b A_f}{\sqrt{C\tau_b\delta_b}} \dfrac{\frac{1}{E_m A_m}\cosh\left(L\sqrt{\frac{C\tau_b}{\delta_b}}\right)+\frac{1}{E_f A_f}}{\sinh\left(L\sqrt{\frac{C\tau_b}{\delta_b}}\right)} > 1, & \text{interfacial debonding} \\ \dfrac{\sigma_f^b A_f}{\sqrt{C\tau_b\delta_b}} \dfrac{\frac{1}{E_m A_m}\cosh\left(L\sqrt{\frac{C\tau_b}{\delta_b}}\right)+\frac{1}{E_f A_f}}{\sinh\left(L\sqrt{\frac{C\tau_b}{\delta_b}}\right)} < 1, & \text{CNT fiber breaking} \end{cases} \tag{8}$$

i.e., a weak interface results in interfacial debonding and fiber pull-out, whereas a strong interface leads to fiber break.

Corresponding to these two failure modes, there are two types of F–δ (pulling force and displacement) curves as shown in Fig. 3a and b, and the corresponding relations are given as follows,

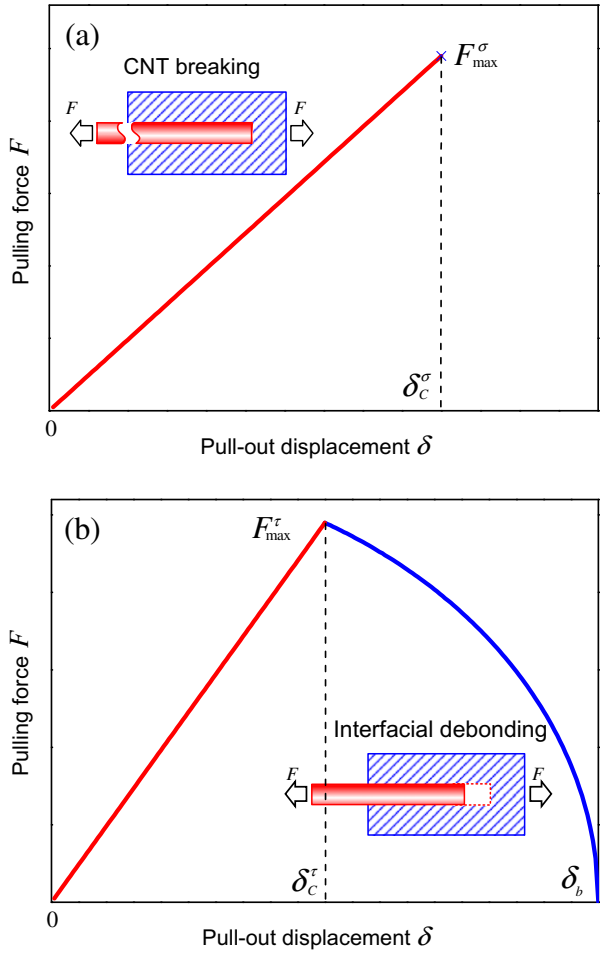

Fig. 3. The relation between the pulling force and the pull-out displacement for the two CNT-fiber failure modes (a) CNT breaking and (b) interfacial debonding.

(iii) CNT break case

$$F = \begin{cases} \delta\sqrt{\frac{C\tau_b}{\delta_b}} \cdot \dfrac{E_f A_f \sinh\left(L\sqrt{\frac{C\tau_b}{\delta_b}}\right)}{\cosh\left(L\sqrt{\frac{C\tau_b}{\delta_b}}\right)+\frac{1}{\alpha}}, & 0 \leqslant \delta \leqslant \delta_C^{\sigma} \\ 0, & \delta > \delta_C^{\sigma} \end{cases} \tag{9}$$

where $\alpha = E_m A_m/(E_f A_f)$ is the stiffness ratio of the matrix to the CNT, and

$$\delta_C^{\sigma} = \sigma_f^b \sqrt{\frac{\delta_b}{C\tau_b}} \cdot \frac{\cosh\left(L\sqrt{\frac{C\tau_b}{\delta_b}}\right)+\frac{1}{\alpha}}{E_f \sinh\left(L\sqrt{\frac{C\tau_b}{\delta_b}}\right)} \tag{10}$$

(iv) CNT pull-out case

$$F = \begin{cases} \delta\sqrt{\frac{C\tau_b}{\delta_b}} \cdot \dfrac{E_f A_f \sinh\left(L\sqrt{\frac{C\tau_b}{\delta_b}}\right)}{\cosh\left(L\sqrt{\frac{C\tau_b}{\delta_b}}\right)+\frac{1}{\alpha}} & 0 \leqslant \delta \leqslant \delta_C^{\tau} \\ E_m A_m \sqrt{\frac{C\tau_b}{\delta_b}\left(\frac{\delta_b^2-\delta^2}{1-\alpha^2}\right)} & \delta_C^{\tau} < \delta \leqslant \delta_b \end{cases} \tag{11}$$

where

$$\delta_C^{\tau} = \delta_b \cdot \left(\alpha + \frac{1-\alpha^2}{\cosh\left(L\sqrt{\frac{C\tau_b}{\delta_b}}\right)+\alpha}\right) \tag{12}$$

It is interesting to note that the curve in Fig. 3b for CNT pull-out case includes both hardening and softening stages.

In CNT-reinforced composites, crack propagation is retarded by the pulling force of the CNTs at the crack surface, which is the so-called "bridge-toughening effect". The displacement of the crack surface (i.e., half of the crack opening displacement) is [37]

$$\delta = \frac{2(1-\nu_m^2)K_{IC}}{E_m}\sqrt{\frac{2r}{\pi}} = \eta K_{IC}\sqrt{r} \tag{13}$$

where r is the distance to the crack tip, and $\eta = 2\sqrt{2}(1-\nu_m^2)/(E_m\sqrt{\pi})$ depends only on Young's modulus E_m and Poisson's ratio ν_m. According to Eq. (9) or (11), the pulling force $F(\delta)$ can be expressed as a function of distance r, i.e., $F(\delta) = F(\delta(r)) = F(r)$. The homogenized traction on the crack surface is then

$$p(r) = F(r)(A_f + A_m)^{-1} \tag{14}$$

and the fracture toughness enhancement ΔK can be computed as [38]

$$\Delta K = \int_0^{\infty} \frac{\sqrt{2}p(r)}{\sqrt{\pi r}}\mathrm{d}r \tag{15}$$

From Eqs. (9)–(15), the fracture toughness enhancement ΔK can be summarized as follows.

$$\Delta K=\begin{cases}\sqrt{\frac{2\delta_b}{\pi C\tau_b}}\frac{(\sigma_f^b)^2A_f}{(A_f+A_m)\eta K_{IC}}\frac{\cosh\left(L\sqrt{\frac{C\tau_b}{\delta_b}}\right)+\frac{1}{2}}{E_f\sinh\left(L\sqrt{\frac{C\tau_b}{\delta_b}}\right)} & \text{(CNT fiber breaking)}\\ \frac{\alpha E_fA_f\sqrt{C\tau_b}\delta_b^{3/2}}{\sqrt{2\pi(1-\alpha^2)}(A_f+A_m)\eta K_{IC}}\left\{\pi-2\arctan\left[\frac{\alpha\cosh\left(L\sqrt{\frac{C\tau_b}{\delta_b}}\right)+1}{\sinh\left(L\sqrt{\frac{C\tau_b}{\delta_b}}\right)\sqrt{1-\alpha^2}}\right]\right\} & \text{(interfacial debonding)}\end{cases} \tag{16}$$

4. Factors affecting the fracture toughness enhancement ΔK and their optimization

Eq. (16) indicates that the fracture toughness enhancement ΔK depends on many factors. Here, we focus on a discussion of the effects of interface length L and interface strength τ_b.

4.1. The effect of interface length L

From the pull-out/break critical condition (Eq. (8)), we know that if $\tau^b < (\sigma_f^bA_f)^2/(CE_m^2A_m^2\delta_b)$, then the failure mode should always be the CNT pull-out, as shown in Fig. 4a. In this case, the fracture toughness enhancement ΔK increases with an increase in interface length L, finally going asymptotically to a constant:

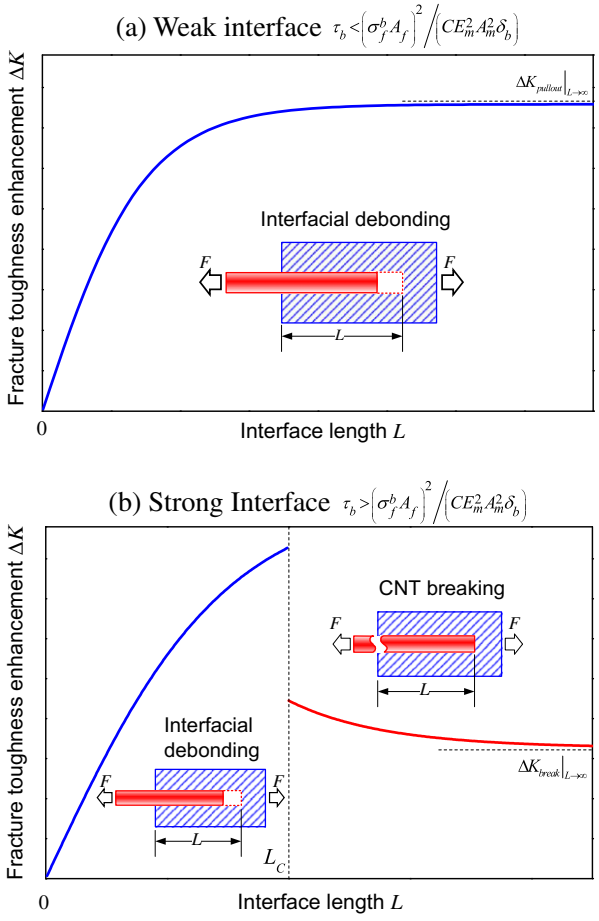

Fig. 4. Schematic diagram for the effect of the interface length on the fracture toughness enhancement, (a) for lower interface strength, the only possible failure mode is interfacial debonding; (b) for higher interface strength, with the increase of the interface length the failure mode converts from interfacial debonding to CNT breaking.

$$\Delta K_{\text{pullout}}|_{L\to\infty}=\sqrt{\frac{C\tau_b}{2\pi}}\frac{E_fA_f\delta_b^{3/2}}{(A_f+A_m)\eta K_{IC}}\frac{\alpha}{\sqrt{1-\alpha^2}}(\pi-2\arcsin\alpha) \tag{17}$$

It is also found that ΔK approaches this asymptotic value quickly with an increase in interface length L, and any further lengthening of the CNTs improves the fracture toughness of the composites only slightly. This is just the case that if only van der Waals interactions are present at the interface of the CNTs and the matrix, the fracture toughening effect is very weak and cannot be improved effectively simply by increasing the CNT length.

For the other case, $\tau_b > (\sigma_f^bA_f)^2/(CE_m^2A_m^2\delta_b)$, as shown in Fig. 4b, a critical length L_C exists and can be determined from the pull-out/break critical condition by Eq. (8):

$$L_C=\sqrt{\frac{\delta_b}{C\tau_b}}\ln\frac{\sigma_f^bA_f\alpha\sqrt{\frac{\delta_b}{C\tau_b}}+\sqrt{(\delta_bE_mA_m)^2-\frac{(\sigma_f^bA_f)^2\delta_b}{C\tau_b}(1-\alpha^2)}}{\delta_bE_mA_m-\sigma_f^bA_f\sqrt{\frac{\delta_b}{C\tau_b}}} \tag{18}$$

When $L < L_C$, the CNT is pulled out, and the fracture toughness enhancement ΔK increases with an increase in interface length L. If L is further increased beyond the critical length L_C, the failure mode is converted from CNT pull-out to CNT break, and ΔK drops significantly. In this regime, the fracture toughness enhancement ΔK decreases with an increase in L, and finally approaches the following value:

$$\Delta K_{\text{break}}|_{L\to\infty}=\sqrt{\frac{2\delta_b}{\pi C\tau_b}}\frac{(\sigma_f^b)^2A_f}{(A_f+A_m)\eta K_{IC}E_f} \tag{19}$$

It is interesting to note that, in this case, lengthening the interface beyond the critical length can even decrease the fracture toughness. Therefore, both cases indicate that improving the composite fracture toughness by increasing the CNT length is effective only for very short CNTs.

4.2. The effect of interface strength τ_b

Another important factor affecting the toughness enhancement is interface strength τ_b, and its effect is shown in Fig. 5. When τ_b is small, the failure mode is CNT pull-out, and the fracture toughness enhancement ΔK increases with an increase in τ_b. Further increasing τ_b beyond the critical interface strength τ_b^c, which can be determined by the pull-out/break critical condition (Eq. (8)), leads the failure mode to be converted from CNT pull-out to CNT break and ΔK to drop significantly. In this regime, the toughness enhancement ΔK decreases with an increase in τ_b. Therefore, for

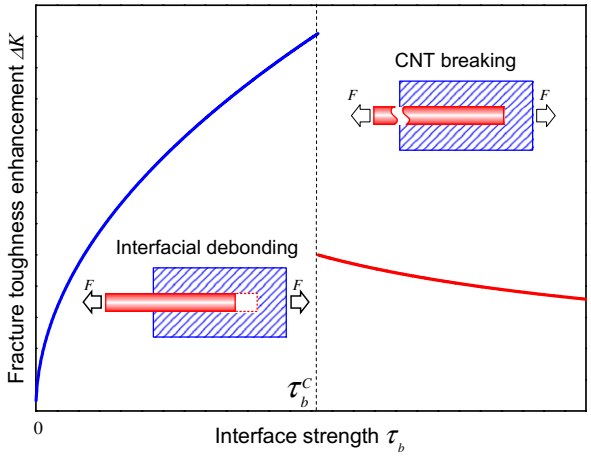

Fig. 5. Schematic diagram for the effect of the interface strength on the fracture toughness enhancement.

CNTs of a given length, the maximum fracture toughness of the composite is achieved when τ_b is only slightly smaller than τ_b^c. This result agrees with the experimental and numerical studies of Xia et al.'s work on ceramic-matrix composites [39,40].

In the following, we attempt to optimize the composite fracture toughness by tailoring both the interface length L and interface strength τ_b, which is essentially a bivariate optimization problem. For convenience, we use another group of variables, normalized interface length $\hat{L} = L\sqrt{C\tau_b/\delta_b}$ and τ_b, instead. According to Eqs. (8) and (16), the maximum ΔK with a given $\hat{L}$ can be achieved when

$$\tau_b = \tau_b^{\text{optimal}}(\hat{L}) = \left(\frac{\sigma_f^b}{E_f}\frac{\frac{1}{\alpha}\cosh(\hat{L})+1}{\sinh(\hat{L})}\right)^2 \Big/ (C\delta_b) \tag{20}$$

Substituting the foregoing expression into Eq. (16) means that the ΔK for the interfacial debonding mode can be expressed as a function of $\hat{L}$ alone, as follows.

$$\Delta K = \frac{\sigma_f^b A_f \delta_b}{\sqrt{2\pi}(A_f + A_m)\eta K_{IC}} \frac{1}{\sqrt{1-\alpha^2}} \times \frac{\cosh(\hat{L})+\alpha}{\sinh(\hat{L})}\left\{\pi - 2\arctan\left[\frac{\alpha\cosh(\hat{L})+1}{\sinh(\hat{L})\sqrt{1-\alpha^2}}\right]\right\} \tag{21}$$

Fig. 6 shows the normalized fracture toughness enhancement $\Delta\hat{K} = \Delta K \cdot \frac{(A_f+A_m)\eta K_{IC}}{\sigma_f^b A_f \delta_b}$ versus $\hat{L}$ for cases with different stiffness ratios: $\alpha = E_m A_m/(E_f A_f)$. It is found that when $\hat{L} \to \infty$, ΔK reaches its optimal value, $\Delta K^{optimal}$, which can be obtained from Eq. (21) as

$$\Delta K^{\text{optimal}} = \Delta K|_{\hat{L}\to\infty} = \frac{\sigma_f^b A_f \delta_b}{(A_f + A_m)\eta K_{IC}} \frac{1}{\sqrt{2\pi(1-\alpha^2)}}(\pi - 2\arcsin\alpha) \tag{22}$$

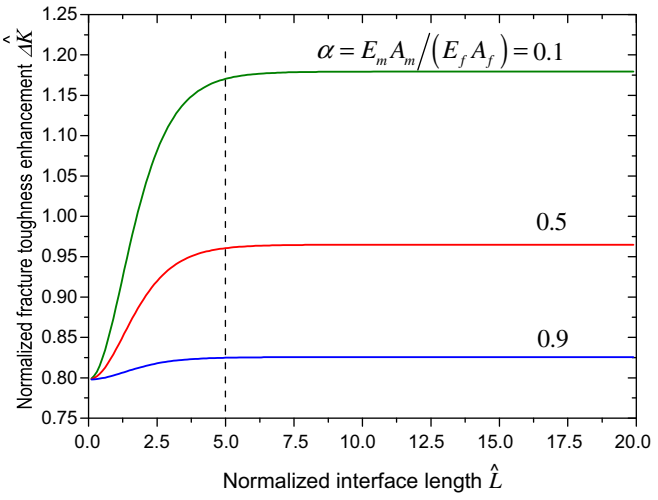

Fig. 6. The normalized fracture toughness enhancement $\Delta\hat{K}$ as a function of the normalized interface length $\hat{L}$ with different stiffness ratio $\alpha = E_m A_m/(E_f A_f)$ and optimal interface strength.

According to Eq. (20), the corresponding optimal interface strength is then

$$\tau_b^{\text{optimal}}\Big|_{\hat{L}\to\infty} = \frac{(\sigma_f^b)^2 A_f}{\pi d \delta_b E_f \alpha(1+\alpha)} \tag{23}$$

It is interesting to note from Fig. 6 that when $\hat{L} > 5$, the difference between ΔK and $\Delta K^{\text{optimal}}$ is less than 1%. Therefore, further increasing the normalized interface length $\hat{L}$ has little effect on the fracture toughness enhancement. Moreover, longer CNTs are more likely to self-fold [41], which dramatically reduces the strength and toughness of the CNT-reinforced composites of which they are a part. We thus suggest that $\hat{L} = 5$ is sufficiently long to achieve good toughness enhancement. For (6,6) CNT-reinforced composites, if the stiffness ratio $\alpha = E_m A_m/(E_f A_f)$ is 1% and only van der Waals interactions are present, then the interface length for $\hat{L} = 5$ is 32.5 nm, and a stronger interface requires only a shorter interface length based on $\hat{L} = L\sqrt{C\tau_b/\delta_b}$. Therefore, 100 nm is sufficiently long, that is, longer CNTs do not further improve the fracture toughness in this case. For CNTs with finite length, we still suggest $\tau_b^{\text{optimal}}\Big|_{\hat{L}\to\infty}$ as the optimal interface strength, since it leads to pull-out failure and is very close to the critical interface strength.

In preparing CNT-reinforced composites, the interface strength τ_b can be tailored by adjusting the interface functionalization bond density, and the statistically mean value of the interface length $\langle L\rangle$ can be controlled by the CNT length l. Suppose that the CNTs are unidirectionally distributed in the matrix. Then, when a macroscopic crack goes through the composite, the bridging CNT is divided into two parts, and the shorter part is likely to be pulled out or break on the crack plane. Since the probabilities of the crack reaching each cross section of the CNT are the same, the average interface length $\langle L\rangle = l/4$.

It should be noted that this fracture toughness optimization method is also suitable for the composites with defective CNTs. Both modulus and strength of the CNTs are reduced due to the defects [42]. Replacing E_f and σ_f^b by reduced values in all the equations, a lower optimal interface strength is obtained comparing with the perfect CNT composites.

5. Computational investigation of atomistic-level failure via the multi-scale finite element method

The analysis in Section 4 indicates that the maximum fracture toughness corresponds to an optimal interfacial chemical bond density that prompts the failure mode to convert from CNT break to CNT pull-out. To verify this result for a CNT-reinforced composite, we adopt a multi-scale FEM in this section. Combined with the continuum FEM, the atomic-scale finite element method (AFEM), which is essentially an effective and accurate molecular statics method [43,44], is employed to account for the interactions between the atoms and the breaking of the chemical bonds accurately.

A (6,6) CNT/polyethylene composite is studied in this paper, and its parameters are given in Table 1. Fig. 7a shows the simulation model. We investigate both CNT-fiber-level failure and the relation between the pulling force F and the pull-out displacement δ. The

Table 1
The parameters of CNT and matrix (polyethylene) in numerical simulation.

CNT		Matrix				
Chirality	Length (nm)	Material	Density ρ (g/cm^3)	E (GPa)	v	Size (nm^3)
(6,6)	7.2	Polyethylene $(-CH_2-)_n$	0.71	2.7	0.3	$4 \times 4 \times 12$

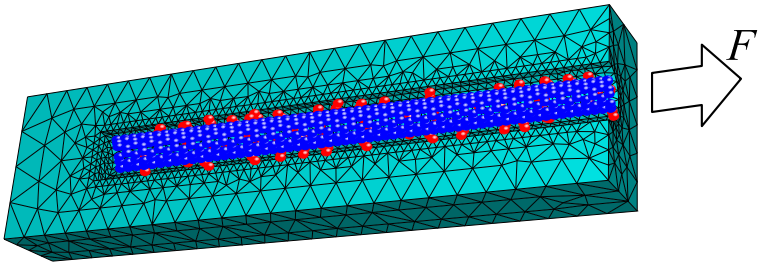

(a)

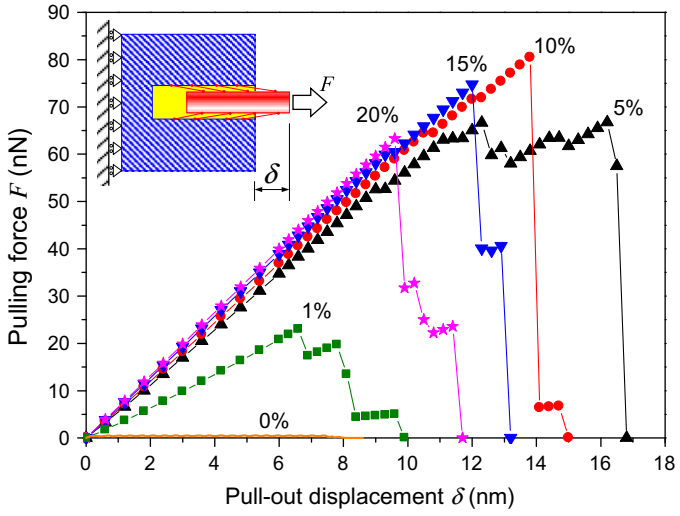

(b)

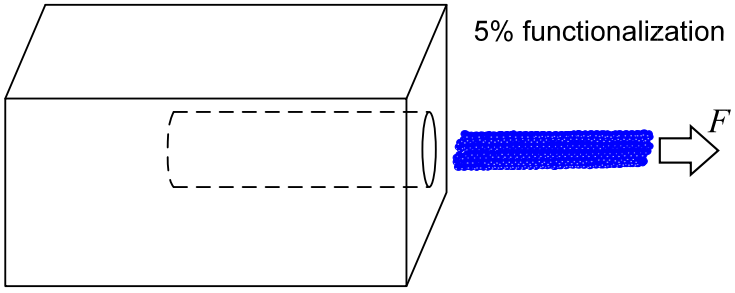

(c)

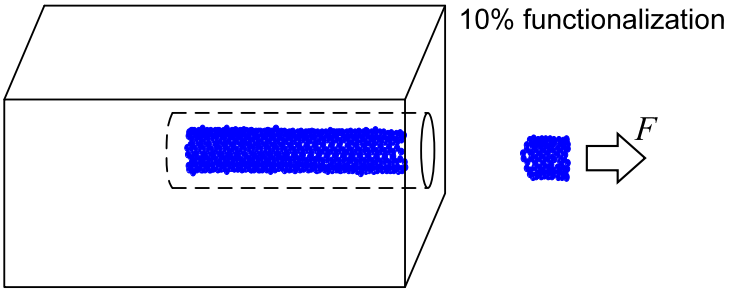

(d)

Fig. 7. (a) Multi-scale simulation model of CNT-pulling problem: 4-node continuum elements for the matrix, and AFEM elements for the CNT and carbon–carbon bond on the interface (the carbon atoms connecting the CNT and the matrix are shown in red); (b) pulling force versus pull-out displacement for the composites with different interfacial chemical bond densities; failure configurations for 5% functionalization (c) and 10% functionalization (d).

continuum FEM is used to simulate the deformation of the matrix, whereas the AFEM is employed to model the failure process of the CNT and the interface. At the atomic-scale level, the interaction at the interface depends on the atom (or atom-group) distributions on the CNT and matrix sides. In our simulation, the atom-groups in the matrix are assumed to be uniformly distributed, and the average distance between the groups is

$$d = \left(\frac{M_{\text{group}}}{\rho_m}\right)^{\frac{1}{3}} \tag{24}$$

where M_{group} is the mass of the atom-group, and ρ_m is the density of the matrix. For the polyethylene investigated in this paper, the average distance between the ($-CH_2-$) groups can be estimated as $d = 0.32$ nm with the mass of the ($-CH_2-$) group and the density of polyethylene. Suppose that the interface is constructed by C–C bonds, and the bonds are distributed randomly on the interface. The interfacial chemical bond density is denoted by the ratio of the bonding atom number to the number of all the atoms on the CNT interface. If the interfacial chemical bond density is absent, only the van der Waals interaction is considered.

As shown in Fig. 7a, the matrix is meshed with node spacing of d on the interface. The interface nodes therefore represent discrete ($-CH_2-$) groups and interact with the CNTs via carbon atoms between them. The interfacial chemical bonding and van der Waals forces are simulated in the AFEM by the second-generation Brenner potential [45] and the Lennard–Jones 6–12 potential [46], respectively. For efficiency, the continuum elements in the matrix farther away from the interface are coarsened gradually.

Fig. 7b shows the relations between the pulling force and pull-out displacement for different interfacial chemical bond densities from the simulation. The CNT-bridging stiffness is represented by the ratio of the pulling force to the pull-out displacement at the initial stage, i.e., the initial slope of the curve in Fig. 7b. It is found that a remarkable improvement in CNT-bridging stiffness occurs when only 1% of the atoms on the surface of the CNT bond with the matrix. This stiffness increases with an increase in bond density, but becomes almost saturated when the bond density goes beyond 5%.

Fig. 7b also indicates that the CNT-bridging strength increases with an increase in bond density when the interfacial chemical density is low, but then decreases when the bond density is higher than 10%. The curves in Fig. 7b exhibit different shapes after the maximum pulling force has been reached, and the atomic configuration is also examined to identify the corresponding failure modes. It is found that when the interfacial chemical bond density falls between 1% and 5%, the entire CNT is pulled out from the matrix, whereas CNT break occurs in the cases of 10%, 15% and 20%. Therefore, when the interfacial chemical bond density is around 5–10%, the failure mode lies just in the transition from interfacial debonding to CNT break, as shown in Figs. 7c and d, which corresponds to the optimal CNT-bridging stiffness, strength and toughness (see Fig. 7b). These results agree well with our theoretical analysis in Section 4.

6. Conclusions

Combining multi-scale simulation, the shear-lag model and fracture mechanics, we have carried out the three-level failure analysis of CNT-reinforced composites, reaching the following conclusions.

(i) Longer reinforced CNTs do not definitely confer better fracture toughness on composites. In a strong CNT/matrix interface, the failure mode is converted from CNT pull-out to CNT break with an increase in CNT length, and the fracture toughness drops suddenly during this transition. In a weak CNT/matrix interface, although the CNT failure mode is CNT pull-out, the fracture toughness improvement due to the reinforced CNTs quickly becomes saturated with an increase in CNT length of hundreds of nanometers at most.

(ii) Stronger CNT/matrix interfaces do not definitely imply that the overall fracture toughness of the composites is better. If the reinforced CNT length is fixed, the failure mode is converted from CNT pull-out to CNT break with an increase in interface strength, and the fracture toughness also declines suddenly during this transition.

(iii) If both the reinforced CNT length and the interface strength can be tailored, keeping in mind that longer CNTs wind, self-fold and cluster more easily, the optimal interface strength and CNT length for maximum fracture toughness are those given in this paper.

Moreover, based on our analysis, we suggest investigating the fractography of CNT-reinforced composites in practical experiments to make an approximate judgment of whether the optimal interfacial chemical bond density and CNT length have been achieved. If most of the CNTs on the fracture section are pulled out, the interfacial chemical bond density or CNT length needs to be increased; if most of these CNTs are broken, in contrast, the interfacial chemical bond density or CNT length needs to be decreased. It should be noted that the theoretical analysis and conclusions drawn in this paper can also be extended to fiber-reinforced composites.

Acknowledgments

The authors acknowledge the support of the National Natural Science Foundation of China (Grant Nos. 10702034, 10732050, 90816006 and 10820101048) and the National Basic Research Program of China (973 Program), Grant Nos. 2007CB936803 and 2010CB832701.

References

[1] Treacy MMJ, Ebbesen TW, Gibson TM. Exceptionally high Young's modulus observed for individual carbon nanotubes. Nature 1996;381:678–80.
[2] Wong EW, Sheehan PE, Lieber CM. Nanobeam mechanics: elasticity, strength, and toughness of nanorods and nanotubes. Science 1997;277:1971–5.
[3] Yu MF, Lourie O, Dyer JM, et al. Strength and breaking mechanism of multiwalled carbon nanotubes under tensile load. Science 2000;287:637–40.
[4] Vigolo B, Pénicaud A, Coulon C, et al. Macroscopic fibers and ribbons of oriented carbon nanotubes. Science 2000;290:1331–4.
[5] Yakobson BI, Campbell MP, Brabec CJ, et al. High strain rate fracture and C-chain unraveling in carbon nanotubes. Comput Mater Sci 1997;8(4):341–8.
[6] Gao GH, Cagin T, Goddard WA. Energetics, structure, mechanical and vibrational properties of single-walled carbon nanotubes. Nanotechnology 1998;9:184–91.
[7] Chen YL, Liu B, Wu J, Huang Y, Jiang H, Hwang K-C. Mechanics of hydrogen storage in carbon nanotubes. J Mech Phys Solids 2008;56:3224–41.
[8] Yin Y, Chen YL, Yin J, Huang KZ. Geometric conservation laws for Y-branched carbon nanotubes. Nanotechnology 2006;17:1–5.
[9] Chen YL, Liu B, Yin Y, Huang Y, Hwang K-C. Nonlinear deformation processes and damage modes of super carbon nanotubes with armchair-armchair topology. Chinese Phys Lett 2008;25(7):2577–80.
[10] Chen YL, Yin Y, Huang Y, Hwang K-C. Atomistic simulations of the nonlinear deformation and damage modes of super carbon nanotubes. J Comput Theor Nanosci 2009;6(1):41–5.
[11] Gojny FH, Nastalczyk J, Roslaniec Z, Schulte K. Surface modified multi-walled carbon nanotubes in CNT/epoxy-composites. Chem Phys Lett 2003;370(5-6):820–4.
[12] Frankland SJV, Caglar A, Brenner DW, et al. Molecular simulation of the influence of chemical cross-links on the shear strength of carbon nanotube-polymer interfaces. J Phys Chem B 2002;106:3046–8.
[13] Frankland SJV, Harik VM. Analysis of carbon nanotube pull-out from a polymer matrix. Surf Sci 2003;525:L103–8.
[14] Ajayan PM, Stephan O, Collies C, Trauth D. Aligned carbon nanotube arrays formed by cutting a polymer resin-nanotube composite. Science 1994;265:1212–4.
[15] Shaffer MSP, Windle AH. Fabrication and characterization of carbon nanotube/poly(vinyl alcohol) composites. Adv Mater 1999;11:937–41.
[16] Gong XY, Liu J, Baskaran S, Voise RD, Young JS. Surfactant-assisted processing of carbon nanotube/polymer composites. Chem Mater 2000;12:1049–52.

[17] Kumar S, Doshi H, Srinivasarao M, et al. Fibers from polypropylene/nano carbon fiber composites. Polymer 2002;43:1701–3.
[18] Tong Y, He XJ, Cheng HM. Effect of carbon nanotubes on mechanical properties and crystallization process of high density polyethylene. New Carbon Mater 2004;19:261–7.
[19] Qian D, Dickey EC, Andrews R, Rantell T. Load transfer and deformation mechanisms in carbon nanotube-polystyrene composites. Appl Phys Lett 2000;76:2868–70.
[20] Bower C, Rosen R, Jin L, Han J, Zhou O. Deformation of carbon nanotubes in nanotube-polymer composites. Appl Phys Lett 1999;74:3317–9.
[21] Ajayan PM, Schadler LS, Giannaris C, Rubio A. Single-walled carbon nanotube-polymer composites: strength and weakness. Adv Mater 2000;12:750–3.
[22] Ni B, Sinnott SB. Tribological properties of carbon nanotube bundles predicted from atomistic simulations. Surf Sci 2001;487:87–96.
[23] Hu Y, Jang I, Sinnott SB. Modification of carbon nanotube-polystyrene matrix composites through polyatomic-ion beam deposition: predictions from molecular dynamics simulations. Compos Sci Technol 2003;63:1663–9.
[24] Yun YH, Dong Z, Shanov VN, Doepke A, Heineman WR, Halsall HB, et al. Fabrication and characterization of carbon nanotube array electrodes with gold nanoparticle tips. Sens Actuators B 2008;133(1):208–12 [28 July].
[25] http://www.nsf.gov/news/news_summ.jsp?cntn_id=108992&org=NSF&from=news.
[26] Cox HL. The elasticity and strength of paper and other fibrous materials. Brit J Appl Phys 1952;3(1):72–9.
[27] Chon T, Sun CT. Stress distributions along a short fibre in fibre reinforced plastics. J Mater Sci 1980;15(4):931–8.
[28] Lawrence P. Some theoretical considerations of fibre pull-out from an elastic matrix. J Mater Sci 1972;7(1):1–6.
[29] Marshall DB, Cox BN, Evans AG. The mechanics of matrix cracking in brittle-matrix fiber composites. Acta Metall 1985;33(11):2013–22.
[30] Hutchinson JW, Jensen HM. Models of fiber debonding and pullout in brittle composites with friction. Mech Mater 1990;9:139–63.
[31] Budiansky B, Evans AG, Hutchinson JW. Fiber-matrix debonding effects on cracking in aligned fiber ceramic composites. Int J Solids Struct 1995;32:315–28.
[32] Shetty DK. Shear-lag analysis of fiber push-out (indentation) tests for estimating interfacial friction stress in ceramic-matrix composites. J Am Ceram Soc 1988;71(2):C107–9.
[33] Bright, JD, Danchaivijit S, Shetty DK. Interfacial sliding friction in silicon carbide–borosilicate glass composites: a comparison of pullout and pushout tests. J Am Ceram Soc 1991; 74(1): 115–22.
[34] Karandikar P, Chou TW. Characterization and modeling of microcracking and elastic moduli changes in nicalon/cas composites. Compos Sci Technol 1993;46(3):253–63.
[35] Nayfeh AH, Abdelrahman WG. Micromechanical modeling of load transfer in fibrous composites. Mech Mater 1998;30(4):307–24.
[36] Starink MJ, Syngellakis S. Shear lag models for discontinuous composites: fibre end stresses and weak interface layers. Mater Sci Eng 1999;A270(2):270–7.
[37] Anderson TL. Fracture mechanics: fundamentals and applications. Boca Raton: CRC Press LLC; 1995.
[38] Tada H, Paris PC, Irwin GR. The stress analysis of cracks handbook. 3rd ed. New York: ASME Press; 2000.
[39] Xia Z, Riester L, Curtin WA, et al. Direct observation of toughening mechanisms in carbon nanotube ceramic matrix composites. Acta Mater 2004;52:931–44.
[40] Xia Z, Curtin WA. Tough-to-brittle transitions in ceramic-matrix composites with increasing interfacial shear stress. Acta Mater 2000;48(20):4879–92.
[41] Zhou W, Huang Y, Liu B, et al. Self-folding of single- and multiwall carbon nanotubes. Appl Phys Lett 2007; 90(7): 73107-1-3.
[42] Zhang ZQ, Liu B, Chen YL, et al. Mechanical properties of functionalized carbon nanotubes. Nanotechnology 2008;19(39):395702.
[43] Liu B, Huang Y, Jiang H, Qu S, Hwang KC. The atomic-scale finite element method. Comput Methods Appl Mech Eng 2004;193:1849–64.
[44] Liu B, Jiang H, Huang Y, et al. Atomic-scale finite element method in multiscale computation with applications to carbon nanotubes. Phys Rev B 2005; 72(3): 35435/1–8.
[45] Brenner DW, Shenderova OA, Harrison JA, Stuart SJ, Ni B, Sinnott SB. A second-generation reactive empirical bond order (REBO) potential energy expression for hydrocarbons. J Phys Condens Matter 2002;14:783–802.
[46] Girifalco L, Hodak AM, Lee RS. Carbon nanotubes, buckyballs, ropes, and a universal graphitic potential. Phys Rev B 2000;62:13104–9.